New Mexico Geological Society

Downloaded from: https://nmgs.nmt.edu/publications/guidebooks/63



U-Pb zircon ages from crustal xenoliths in a Pliocene basalt flow from the southern Rio Grande rift: Implications for the timing of extension and magmatism

Jeffrey M. Amato, Carmen Athens, William C. McIntosh, and Lisa Peters
2012, pp. 273-284. https://doi.org/10.56577/FFC-63.273

in:

Geology of the Warm Springs Region, Lucas, Spencer G.; McLemore, Virginia T.; Lueth, Virgil W.; Spielmann, Justin A.; Krainer, Karl, New Mexico Geological Society 63rd Annual Fall Field Conference Guidebook, 580 p. https://doi.org/10.56577/FFC-63

This is one of many related papers that were included in the 2012 NMGS Fall Field Conference Guidebook.

Annual NMGS Fall Field Conference Guidebooks

Every fall since 1950, the New Mexico Geological Society (NMGS) has held an annual Fall Field Conference that explores some region of New Mexico (or surrounding states). Always well attended, these conferences provide a guidebook to participants. Besides detailed road logs, the guidebooks contain many well written, edited, and peer-reviewed geoscience papers. These books have set the national standard for geologic guidebooks and are an essential geologic reference for anyone working in or around New Mexico.

Free Downloads

NMGS has decided to make peer-reviewed papers from our Fall Field Conference guidebooks available for free download. This is in keeping with our mission of promoting interest, research, and cooperation regarding geology in New Mexico. However, guidebook sales represent a significant proportion of our operating budget. Therefore, only *research papers* are available for download. *Road logs*, *mini-papers*, and other selected content are available only in print for recent guidebooks.

Copyright Information

Publications of the New Mexico Geological Society, printed and electronic, are protected by the copyright laws of the United States. No material from the NMGS website, or printed and electronic publications, may be reprinted or redistributed without NMGS permission. Contact us for permission to reprint portions of any of our publications.

One printed copy of any materials from the NMGS website or our print and electronic publications may be made for individual use without our permission. Teachers and students may make unlimited copies for educational use. Any other use of these materials requires explicit permission.

This page is intentionally left blank to maintain order of facing pages.

U-PB ZIRCON AGES FROM CRUSTAL XENOLITHS IN A PLIOCENE BASALT FLOW FROM THE SOUTHERN RIO GRANDE RIFT: IMPLICATIONS FOR THE TIMING OF EXTENSION AND MAGMATISM

JEFFREY M. AMATO[1], CARMEN ATHENS[1], WILLIAM C. McINTOSH[2] AND LISA PETERS[2]
[1]Department of Geological Sciences, New Mexico State University, Las Cruces, New Mexico, 88003; amato@nmsu.edu
[2]Department of Earth and Environmental Sciences, New Mexico Institute of Mining and Technology, Socorro, New Mexico, 87801

Abstract—Metaigneous xenoliths with granulite facies assemblages from the Pliocene Elephant Butte volcanic field basalts flows were derived from the lower crust. Protolith compositions are inferred to be diorite and granite based on mineralogy and color index. The metadiorite has orthopyroxene (opx) compositions of En_{68}–En_{55} and plagioclase compositions of An_{48}–An_{45}, whereas the metagranite has opx compositions of En_{55}–En_{30} and plagioclase compositions of An_{40}–An_{35}. Augite is also more magnesian in the metadiorite relative to the metagranite. A $^{40}Ar/^{39}Ar$ date on the host basalt is 2.71 ± 0.06 Ma. Cathodoluminescence imaging indicates that xenolith zircons have both oscillatory zoned cores as well as altered cores and low-U rims. The core dates are complicated by high common Pb and discordance, but the best core ages from the four samples dated are 1664 ± 14 Ma, 1452 ± 32 Ma, ~1450 Ma, and 1432 ± 14 Ma. The core age of 1664 Ma is similar to other dates from Mazatzal province basement, and the ~1450 Ma dates from the remaining samples is similar to other dates from surface exposures of granites that are part of the ~1.4 Ga granite-rhyolite province. These dates indicate that ~1.4 Ga granites are found at all depths of the crust indicating a significant volume of ~1.4 Ga granite in the crust. The rim dates for two samples are similar at 9.8 ± 1.7 Ma and 11.0 ± 2.2 Ma. A combined age using three samples is 10.4 ± 1.1 Ma. This age is coeval with the Selden basalt flow >60 km to the south and coincides with the onset of extension and magmatism following a 8 m.y. hiatus. The lack of surface flows at 10 Ma at Elephant Butte suggests that mantle derived magmas provided heat to the lower crust, possibly by underplating, but that extension was not yet significant enough to allow magmatism to occur. Volcanism at 2.7 Ma at Elephant Butte brought up the xenoliths and was facilitated by extension in the transfer zone between two offset north-striking and west-dipping normal faults. The Miocene zircon rim ages in Proterozoic xenoliths provide indirect evidence for the onset of extension-related heating of the lower crust in the absence of surface eruptions.

INTRODUCTION

Crustal xenoliths have long been recognized as a way to glean valuable information about the composition, age, and conditions of the lower crust (e.g., Kay and Kay, 1981; Hanchar et al., 1994). Zircons from crustal xenoliths can reveal multiple episodes of igneous and metamorphic growth (Hanchar and Rudnick, 1995), and using cathodoluminescence (CL) images of the zircons to guide spot dating using SHRIMP (sensitive high-resolution ion microprobe) is a powerful method to determine the U-Pb ages of these different episodes.

In the southern Rio Grande rift (Fig. 1; Chapin, 1971), rift-related magmatism over the last ~30 m.y. has been used to evaluate the relationship between magmatism and extension (e.g., Seager et al., 1984; Mack, 2004), and mafic volcanism has been used to evaluate the evolution of the mantle beneath the rift (e.g., Perry et al., 1987; McMillan et al., 2000). The total volume of erupted material since 10 Ma is relatively small, and this may correlate with the modern slow spreading rate determined using geophysical data (Berglund et al., 2012).

Whereas exposed Proterozoic crust along the Rio Grande rift and adjacent fault blocks can be evaluated in context, xenoliths provide direct sampling of otherwise unobservable lower crust. These rocks may be part of the source rocks for 1.4 Ga granitic magmatism or they may be themselves part of the 1.4 Ga igneous event. Other igneous or metamorphic events may be recorded in zircon growth within the xenoliths.

The goal of this paper is to provide new ages of the host basalt and from lower crustal granulite facies xenoliths and use them to better understand the composition of Proterozoic crust as well as to determine the ages of subsequent crustal events including the history of magmatism in the Rio Grande rift.

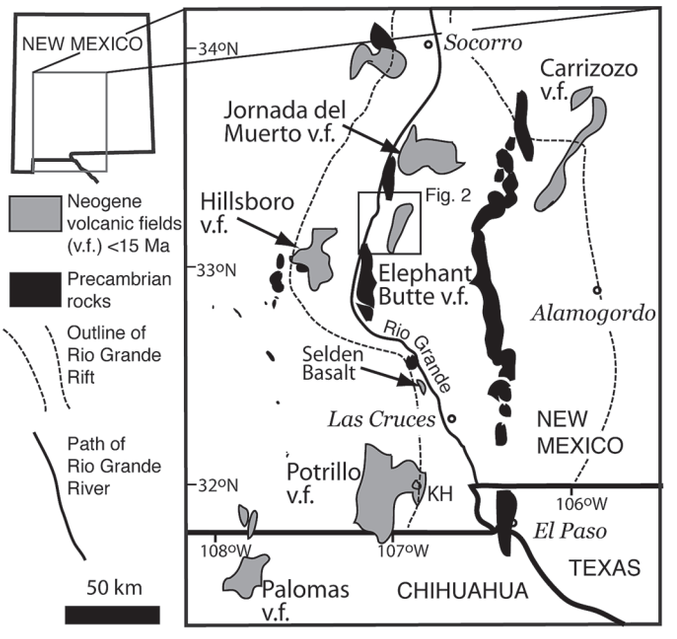


FIGURE 1. Location map of south-central New Mexico showing the distribution of Precambrian rocks and Neogene volcanic fields. Also shown is the outline of the Rio Grande rift (Chapin, 1971). After Baldridge (2004). KH=Kilbourne Hole.

REGIONAL GEOLOGY

The Fra Cristobal Mountains and Cutter Sag areas (Fig. 2) are part of the Mazatzal province that consists of igneous basement of likely arc origin that ranges in age from 1.7–1.6 Ga and have juvenile isotopic geochemical signatures (Karlstrom et al., 2004). The Mazatzal orogeny began around 1.65 Ga and records the accretion of the Mazatzal province to the Yavapai province along a NE-trending suture near the New Mexico-Colorado border (Karlstrom and Bowring, 1988; Amato et al., 2008). Rock types within the largest exposure of Mazatzal province crust in southern New Mexico, the Burro Mountains, include amphibolite, gabbro, orthogneiss, metarhyolite, and metasedimentary rocks including schist and quartzite (Amato et al., 2008; 2011).

Granitic plutons and rhyolites ranging in age from 1,490–1,340 Ma are found in a wide belt across North America (Anderson, 1989; Anderson and Morrison, 2005; Amato et al., 2011). These have been referred to as "A-type" granites. In the Burro Mountains, these plutons include granodiorite and granite; they intruded at 1470–1460 Ma (Amato et al., 2011). New U-Pb dates from the Caballo Mountains are presented in Amato and Becker (thiseguidebook) and indicate magmatism at around 1480 Ma.

The Rio Grande rift is a narrow continental rift that extends >1,000 km from central Colorado to west Texas (Wilson et al., 2005a). The onset of extension is proposed to have coincided with eruption of the ~35 Ma tuffs of the Bell Top Formation (McMillan et al., 2000), although others have suggested that this magmatism was related to subduction that accompanied the Laramide orogeny and that rifting began later (Henry and Price, 1986). Mafic volcanism in southern New Mexico began with the eruption of the Uvas basaltic andesites at ~28–26 Ma and this event was interpreted by Seager et al. (1984) as reflecting the onset of rifting. Regardless of the actual beginning of rifting, this initial stage continued until about 18 Ma (Seager et al., 1984).

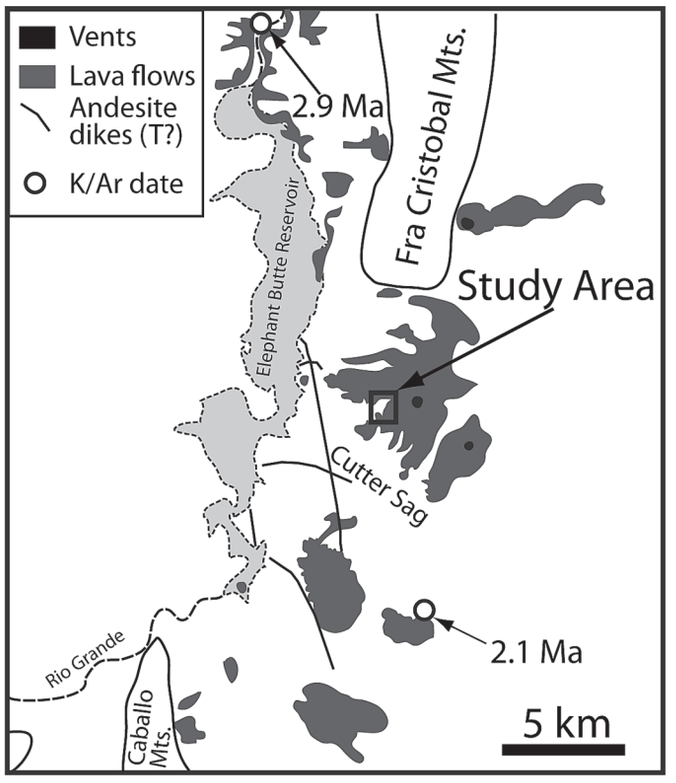


FIGURE 2. Simplified geologic map of the Elephant Butte volcanic field flows and vents. The previously published K/Ar dates shown are from Bachman and Mehnert (1978). Distribution of volcanic rocks is from Google Earth and Harrison and Cather (2004).

The second stage of rifting and magmatism began after a 10 m.y. hiatus. This phase began with the eruption of the Selden basalt (Fig. 1) at 9.6 Ma (Seager et al., 1984) and resulted in Basin and Range style block faulting (Keller et al., 1991). Other Neogene basalt flows erupted from ~5–2 Ma, including the ~3–2 Ma basalts of the Elephant Butte volcanic field that are part of this study (see summary in Mack, 2004). Holocene basalt eruptions (Fig. 1) include the 20,000 year old eruption at the Kilbourne Hole maar within the Potrillo volcanic field (Anthony and Poths, 1992), and the ~5000 year old Carrizozo flow (Dunbar, 1999).

The Kilbourne Hole locality (Fig. 1) has a diverse suite of both mantle and crustal xenoliths, including garnet granulites from the lower crust indicating depths of ~28 km (Padovani and Carter, 1977; Scherer et al., 1997). SHRIMP dating of zircons from these xenoliths yielded a wide range of ages (Archean to Phanerozoic) with multiple ages around 75 Ma, 35 Ma, 26 Ma, 5.5 Ma, and 2.7 Ma (Liati and Gebauer, 2002). Xenoliths at Potrillo maar yielded U-Pb zircon ages of 1.07 Ga and 26 Ma (Li et al., 2004) and have been used to construct a geologic and seismic profile of the crust beneath the southern Rio Grande rift (Hamblock et al., 2007). The xenoliths from the Elephant Butte field have not previously been dated.

GEOLOGY OF THE FRA CRISTOBAL MOUNTAINS AND CUTTER SAG

The Cutter Sag area, where the Elephant Butte volcanic field is located, lies between the Fra Cristobal Mountains, the Caballo Mountains, and the Elephant Butte Reservoir (Fig. 2). The study area is part of the privately owned Armendaris Ranch. Previous geologic studies of the area include Kelley and Silver (1952), Thompson (1955a, b), Nelson and Hunter (1986)G. H. and Lozinsky (1986). Mack and Seager (1995) interpreted Cutter Sag as a transfer zone between synthetic normal faults of the Rio Grande Rift and that this faulting was responsible for the abundant basaltic volcanism. These basalts form the Elephant Butte volcanic field. One basalt from about 10 km SSW of the study area was previously dated with a K-Ar whole-rock date of 2.1 ± 0.4 Ma (2σ uncertainty), and another sample from 15 km NNE of the study area yielded a K-Ar date of 2.9 ± 0.3 Ma (Bachman and Mehnert, 1978). Warren et al. (1979) analyzed the geochemistry of various xenoliths in the Pliocene basalts just east of Elephant Butte Reservoir and discovered lherzolite, pyroxenite, two-pyroxene granulite, biotite granite, and megacrysts of clinopyroxene, olivine, plagioclase, and spinel. These were inferred to originate from depths of 29–36 km at ~900-1100 °C for granulite and pyroxenite and 36 to >42 km at 1100–1200 °C for lherzolite (Warren et al., 1979).

METHODS

All samples were collected from a basalt flow at the drainage at UTM 13S, 302750E, 3678590N (datum WGS84). They were generally from within the lowest part of the lowest flow that overlies Cretaceous sandstone.

Mineral compositions were investigated at the New Mexico Institute of Mining and Technology using a Cameca SX-100 electron microprobe with 3 wavelength dispersive (WD) spectrometers. Samples were examined using backscattered electron (BSE) imagery, and selected particles were quantitatively analyzed. Elements analyzed include F, Na, Mg, Al, Si, P, S, Cl, K, Ca, Ti, Cr, Mn, Fe, Sr and Ba. An accelerating voltage of 15 kV and probe current of 20 nA was used with the exception of analyses of glass which utilized a 10 nA probe current. Peak count times of 20 s were used for all elements with the exception of F (40 s (amph); 60 s (glass)), Cl (40 s), S (30 s), Sr (60 s), and Ba (60 s). Background count times were one half the peak count times. A point beam (1 μm) was used for analyses of amphibole, pyroxene and Fe oxide (Table 1). A slightly defocused beam was used for analyses of feldspar (10 μm), glass and carbonate (20 μm) to avoid losses due to sodium volatilization (Nielsen and Sigurdsson, 1981) (Table 2). Standard reference materials, including feldspars, amphiboles and Fe-Ti oxides were run as unknowns in each analytical session to monitor calibration accuracy and inter-run reproducibility. Data reduction was undertaken using a ZAF procedure.

The host basalt was dated by the $^{40}Ar/^{39}Ar$ incremental-heating method at the New Mexico Geochronology Research Laboratory. The samples were irradiated in a machined aluminum tray at the U.S. Geological Survey TRIGA reactor in Denver, Colorado. The neutron flux monitor was the Fish Canyon Tuff sanidine (FC-2) with an assigned age of 28.02 Ma (Renne et al., 1998). The analyses were performed on a Mass Analyzer Products 215-50 mass spectrometer on line with an automated all-metal extraction system. Flux monitors and samples were step-heated by a 50 watt Synrad CO_2 laser. J-factors were determined by laser-fusion of six single crystals from each of six radial positions around the irradiation tray. Decay constants and isotopic abundances were from Steiger and Jäger (1977), and the plateau age errors are based on Taylor (1982). Other details of the analytical methods are in the footnote to Table 3.

U-Pb geochronology (Table 4) was carried out using the SHRIMP-RG (sensitive high-resolution ion microprobe reverse geometry) at the Stanford–U.S. Geological Survey Ion Probe Facility. Beam diameter was 30 mm. All errors reported in the text are at 2σ, but the ages on individual spot ages are reported at 1σ in the text and tables. Details of the SHRIMP methods are in Amato et al. (2008). Analyses of young (<20 Ma) zircons indicated high concentrations of common Pb. For these analyses, we used the technique of calculating $^{206}Pb/^{238}U$ model ages based on the intercept of a regression line on a Tera-Wasserberg concordia diagram (e.g., Schmitt et al., 2003; Schmitt and Hulen, 2008) fixed to a modern common Pb composition in which $^{207}Pb/^{206}Pb$ =0.82 ± 0.02 (Sanudo-Wilhelmy and Flegal, 1994). Other U-Pb data are shown on conventional concordia diagrams, relative probability plots, and weighted mean plots (Ludwig, 2008). Most samples were relatively small, yet yielded a surprisingly large number of zircons, with some samples yielding >100 individual zircon grains.

Table 1. Pyroxene Compositions

Point	SiO_2	Al_2O_3	MgO	FeO	MnO	TiO_2	CaO	Na_2O	Total
AR-03: Orthopyroxene									
14	32.2	0.0	13.3	55.3	1.0	0.1	0.3	0.0	102.2
15	33.1	0.0	16.3	52.4	0.9	0.0	0.4	0.1	103.3
9	50.2	3.1	17.8	28.8	1.2	0.2	1.3	0.1	102.5
17	50.1	2.1	17.7	29.4	1.2	0.2	1.3	0.1	102.0
12	50.1	2.1	17.6	29.1	1.2	0.2	1.3	0.1	101.7
10	50.2	2.0	17.7	29.0	1.2	0.2	1.3	0.1	101.5
28	50.2	2.0	17.6	29.1	1.2	0.2	1.4	0.1	101.6
16	51.3	1.0	18.2	26.9	1.0	0.2	2.8	0.1	101.4
13	51.0	1.3	17.8	27.5	0.9	0.2	2.9	0.1	101.6
AR-03: Clinopyroxene									
25	50.5	1.2	11.4	21.3	0.6	0.4	15.9	0.3	101.4
24	48.8	1.6	6.6	26.4	0.5	0.3	17.1	0.3	101.8
26	49.6	3.5	11.3	15.7	0.8	0.4	18.2	0.8	100.3
27	49.4	3.4	11.0	15.7	0.7	0.4	18.2	0.8	99.7
20	49.4	3.4	11.1	15.5	0.7	0.4	18.3	0.7	99.5
19	49.8	1.6	10.7	18.2	0.4	0.3	18.6	0.3	99.9
AR-04: Orthopyroxene									
21	36.9	0.0	31.8	32.4	0.8	0.0	0.3	0.0	102.1
37	37.1	0.0	32.1	32.3	0.7	0.0	0.3	0.0	102.6
33	37.6	0.1	34.1	30.1	0.7	0.0	0.4	0.0	103.0
38	37.2	0.0	33.0	31.3	0.6	0.0	0.4	0.0	102.6
18	36.8	0.1	33.0	30.4	0.6	0.0	0.5	0.1	101.5
14	38.2	1.0	32.2	28.6	0.6	0.2	0.6	0.3	101.7
34	36.8	0.4	28.1	33.1	0.7	0.0	0.6	0.1	99.7
10	35.3	1.2	23.5	35.1	0.6	0.0	0.8	0.1	96.4
29	51.0	3.2	21.8	23.3	0.6	0.1	1.1	0.1	101.2
13	51.0	3.2	21.9	22.9	0.6	0.2	1.1	0.1	100.8
28	50.9	3.4	21.8	23.3	0.7	0.2	1.1	0.1	101.4
32	50.8	3.5	21.8	23.5	0.6	0.2	1.1	0.1	101.5
12	51.1	3.1	21.9	23.1	0.6	0.2	1.1	0.1	101.2
AR-04: Clinopyroxene									
15	52.9	1.1	17.1	10.9	0.4	0.4	16.9	0.5	100.2
11	53.8	1.3	16.0	10.3	0.4	0.3	16.9	0.7	99.7
19	53.2	0.8	16.7	10.6	0.4	0.3	17.9	0.5	100.3
20	53.2	0.7	16.8	10.3	0.4	0.4	18.2	0.5	100.5
35	53.6	2.2	16.2	10.9	0.5	0.4	18.4	0.6	102.8
39	53.6	3.4	16.3	10.0	0.4	0.4	19.0	0.6	103.6
30	50.0	4.8	12.5	12.2	0.3	0.6	19.3	0.9	100.5
24	49.2	3.5	15.1	9.8	0.2	1.7	19.4	0.5	99.4
2	49.4	4.8	12.4	12.2	0.4	0.6	19.5	0.8	100.0
8	49.3	4.8	12.3	12.2	0.3	0.6	19.5	0.9	99.9
9	49.4	4.8	12.4	12.0	0.4	0.5	19.5	0.9	99.9
1	49.4	4.9	12.2	12.1	0.4	0.6	19.6	0.9	100.0
36	53.2	0.7	16.1	9.3	0.3	0.4	20.0	0.5	100.5
3	49.6	3.2	13.9	8.6	0.1	1.8	21.8	0.8	99.7
4	50.6	2.6	14.1	8.8	0.2	1.1	22.1	0.7	100.1

Note: All concentrations are in oxide weight %

Table 2. Feldspar Compositions

Point	SiO_2	Al_2O_3	Na_2O	K_2O	CaO	FeO	SrO	BaO	Total
AR-03-Alkali Feldspar									
8	66.7	17.9	6.0	7.7	0.1	0.5	0.0	0.1	99.1
10	67.4	18.5	7.5	6.0	0.2	0.6	0.1	0.1	100.4
9	64.2	20.2	3.5	10.5	0.7	0.2	0.1	1.4	100.7
8	64.2	20.1	3.7	10.6	0.8	0.2	0.1	1.4	100.9
7	64.3	20.1	3.7	10.3	0.8	0.2	0.1	1.2	100.7
12	64.4	20.2	3.7	10.5	0.9	0.2	0.1	1.4	101.3
5	65.1	20.4	6.6	6.0	0.9	0.1	0.0	1.6	100.9
6	65.4	20.7	6.4	6.3	0.9	0.2	0.1	1.5	101.4
11	65.8	20.6	6.7	5.7	1.2	0.2	0.1	1.4	101.6
10	65.9	20.9	7.0	4.5	1.5	0.2	0.1	1.5	101.6
AR-03-Plagioclase Feldspar									
3	59.3	24.3	6.7	1.8	6.5	0.3	0.1	0.1	99.1
11	59.2	24.4	6.5	1.8	6.6	0.3	0.1	0.1	99.0
4	59.1	24.6	7.0	1.1	6.7	0.4	0.1	0.0	98.9
12	58.7	24.6	6.2	1.7	7.0	0.3	0.1	0.1	98.6
6	59.1	24.7	6.2	1.6	7.0	0.4	0.1	0.1	99.1
7	59.4	24.6	6.5	1.5	7.1	0.4	0.1	0.1	99.6
5	58.9	24.8	6.4	1.6	7.2	0.3	0.1	0.1	99.4
9	59.0	24.9	6.9	1.0	7.3	0.4	0.1	0.1	99.6
AR-04-Plagioclase Feldspar									
13	56.1	26.5	5.8	0.7	9.2	0.4	0.2	0.1	99.0
14	56.1	26.7	5.8	0.7	9.0	0.4	0.3	0.1	99.0
15	55.7	26.5	5.7	0.7	8.8	0.4	0.3	0.0	98.0
16	55.7	26.8	5.9	0.7	9.1	0.3	0.3	0.1	98.8
17	55.7	26.8	5.9	0.7	8.9	0.4	0.2	0.0	98.7

Note: All concentrations are in oxide weight %

SAMPLES DATED

Xenolith samples are all granulite facies metamorphic rocks based on the presence of two pyroxenes and the absence of hydrous minerals such as biotite or amphibole. The samples include AR-1, which is approximately 6 cm by 5 cm and consists of quartz, K-feldspar with exsolution lamellae, plagioclase, orthopyroxene, and clinopyroxene (Fig. 3). Clinopyroxene is restricted to a <1 mm wide vein running through the xenolith (Fig. 4). It is unclear whether this vein is related to the host basalt magma or if it is an older feature. The crystals are equant with polygonal shapes Fig. 4). The rock has a strong foliation of alternating dark and light minerals. Sample AR-2 is approximately 4 cm by 3 cm; a thin-section was not made because of its small size, but macroscopic evaluation indicates the presence of quartz, feldspar, and pyroxene. The rock has a weak foliation. Sample AR-3 is approximately 3 cm by 2 cm and is leucocratic with quartz, microcline, plagioclase, orthopyroxene, and clinopyroxene. The sample has a weak foliation. Additional phases identified using electron microprobe include ilmenite, apatite, titanomagnetite. Sample AR-4 is approximately 4 cm by 5 cm and consists of plagioclase clinopyroxene, orthopyroxene, and quartz. No zircons were recovered from this sample. The sample has a weak foliation. Sample AR-5 is approximately 3 cm by 5 cm and is leucocratic with quartz, plagioclase, clinopyroxene, and zircon. The sample has a weak foliation.

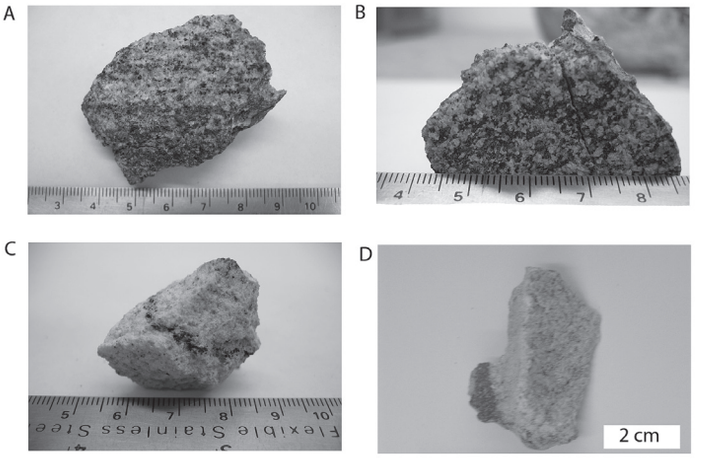


FIGURE 3. Photographs of hand samples of xenoliths before they were crushed for geochronology. Samples include (A) AR-1; (B) AR-2; (C) AR-3; (D) AR-5. Sample AR-4 had no zircons and was not photographed. Scale in A–C is in cm.

The host basalt (sample AR-8) has phenocrysts of olivine with iddingsite cores, clinopyroxene, and orthopyroxene with a groundmass of microlite plagioclase and Fe-Ti oxides. Vesicles are present, as are clusters of fine pyroxene and olivine interpreted as microxenoliths of mantle origin. Zircons are visible in thin section.

GEOCHEMISTRY AND MINERAL TEXTURES

Two samples were analyzed on the electron microprobe for mineral compositions and textures. Sample AR3 has a texture that is a fine symplectic intergrowth of plagioclase and orthopyroxene (Fig. 5). Sample AR4 has orthopyroxene crystals with a composition of En_{62} found in the core with a rim that has reacted to a symplectic intergrowth of orthopyroxene (En_{66}) and clinopyroxene (generally $En_{47}Fs_{36}Wo_{17}$) (Table 1). The orthopyroxene from sample AR-03 ranges from En_{30} to En_{55}, whereas the opx from sample AR-04 is more magnesian, ranging from En_{55} to En_{68}. This pattern of more magnesian compositions is observed also from clinopyroxenes, with sample AR-03 having compositions ranging from $En_{20}Fs_{48}Wo_{32}$ to $En_{34}Fs_{27}Wo_{39}$ and sample AR-04 having cpx compositions ranging from $En_{37}Fs_{21}Wo_{43}$ to $En_{46}Fs_{16}Wo_{38}$. Plagioclase compositions in sample AR-03 are ~An_{35}-An_{40} whereas those from sample AR-04 are around An_{45}-An_{48} (Table 2).

FIGURE 4. Scanned images of thin sections from xenoliths. Samples include (A) AR-1; (B) AR-3; (C) AR-4; (D) AR-5. Sample AR-2 not cut for a thin section. Width of each area imaged is approximately 1.5 cm.

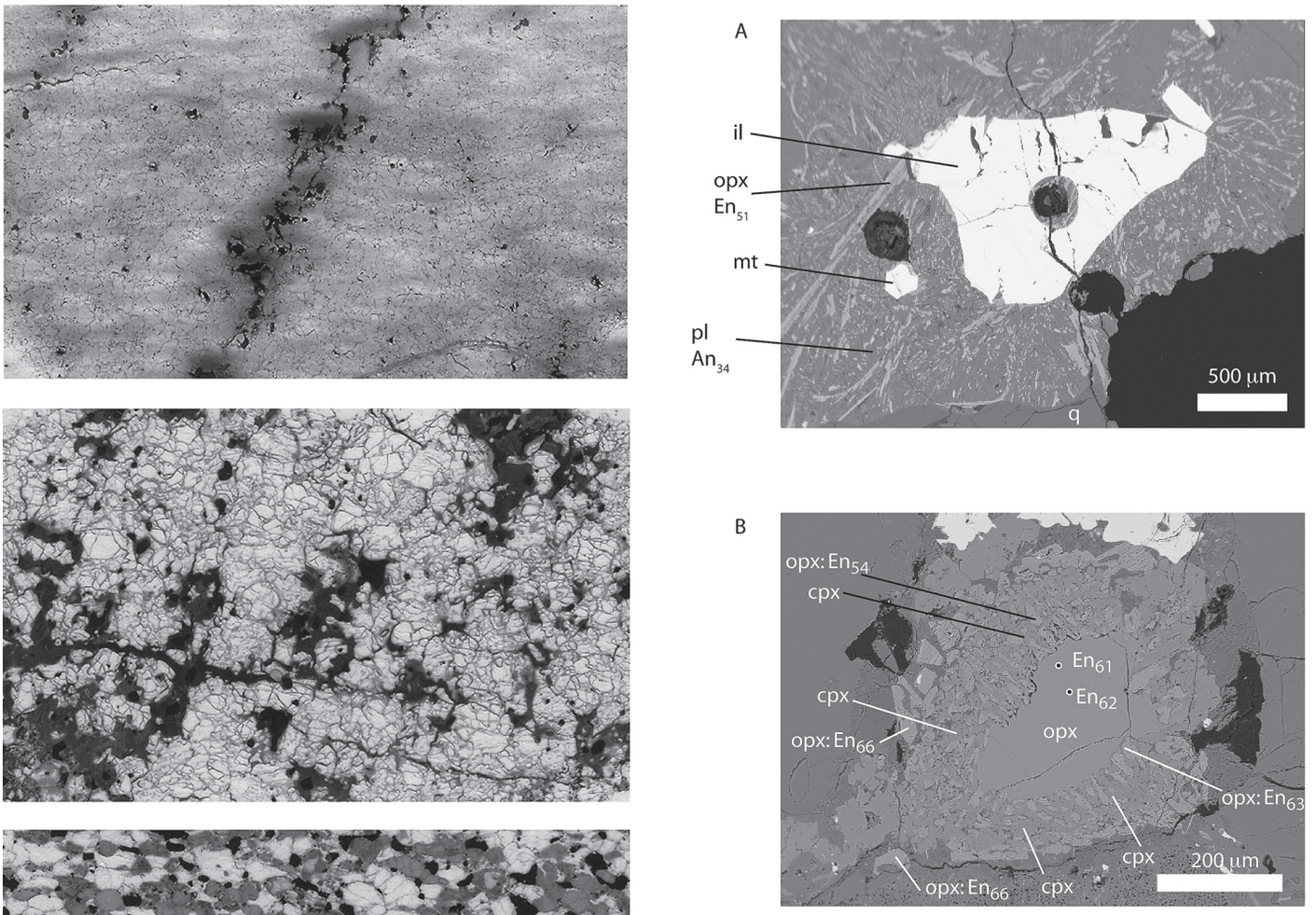


FIGURE 5. Scanning electron microscope back-scattered electron images and mineral compositions of plagioclase (An) and orthopyroxene (En) from (A) sample AR-3, showing symplectic intergrowth of plagioclase and orthopyroxene; and (B) sample AR-4, showing symplectic intergrowth of orthopyroxene and clinopyroxene. Mineral abbreviations: il, ilmenite; opx, orthopyroxene; cpx, clinopyroxene; mt, magnetite; pl, plagioclase; q, quartz;

GEOCHRONOLOGY RESULTS

We obtained a $^{40}Ar/^{39}Ar$ date on the host basalt (sample 05AR-8). The sample dated was a groundmass concentrate representative of the whole-rock without phenocrysts. Eight heating steps were analyzed and the lowest-temperature step was younger and not used in the age calculation (Fig. 6; Table 3). The remaining seven steps yielded a weighted mean age of 2.71 ± 0.06 Ma (error is quoted at 2σ; MSWD=2.7). This plateau age is within error of the isochron age of the sample (2.74 ± 0.08 Ma) that had a $^{40}Ar/^{36}Ar$ intercept at 294 ± 4, a value that is within error of the atmospheric ratio of 295.5.

Zircons from the xenoliths have a range of textures. As shown on cathodoluminescence (CL) images, in which bright zones in CL indicate low U and dark zones indicate high U, most grains have cores with different CL intensities than the rims. Cores in

Table 3. $^{40}Ar/^{39}Ar$ analytical data.

ID	Temp (°C)		$^{40}Ar/^{39}Ar$	$^{37}Ar/^{39}Ar$	$^{36}Ar/^{39}Ar$ (x 10-3)	^{39}ArK (x 10-15 mol)	K/Ca	$^{40}Ar^*$ (%)	^{39}Ar (%)	Age (Ma)	±1σ (Ma)
05AR-8, Groundmass Concentrate, 32.02 mg, J=0.0007833±0.09%, D=1.0068±0.0015, NM-208H, Lab#=57166-01											
X A	3		3215.9	1.101	10962.4	0.137	0.46	-0.7	0.1	-33.41	30.94
X B	3		121	0.7099	408.8	2.954	0.72	0.2	1.2	0.38	1.15
C	4		14.99	0.7274	43.79	16.32	0.7	14.1	7.8	2.98	0.14
D	4		5.481	0.5194	12.11	40.6	0.98	35.5	24.3	2.75	0.04
E	5		3.988	0.5376	6.989	45.8	0.95	49.3	43.4	2.78	0.03
F	6		4.383	0.6929	8.694	30.48	0.74	42.7	56.3	2.64	0.04
G	8		5.883	1.147	13.9	40.63	0.44	31.8	73.9	2.64	0.05
H	10		6.287	2.581	15.69	30.56	0.2	29.6	87.3	2.64	0.06
I	25		6.999	5.193	18.6	28.3	0.098	27.6	100	2.74	0.07
Integrated age ± 2σ		n=9				235.8	0.34		K_2O=3.61%	2.67	0.14
Plateau ± 2σ	steps C-I	n=7			MSWD=2.70	232.7	0.62 ±0.70		98.7	2.71	0.06
Isochron±2σ	steps A-I	n=9			MSWD=2.76		$^{40}Ar/^{36}Ar$=293.6±4.0			2.74	0.08

Notes:

Isotopic ratios corrected for blank, radioactive decay, and mass discrimination, not corrected for interfering reactions.

Errors quoted for individual analyses include analytical error only, without interfering reaction or J uncertainties.

Integrated age calculated by summing isotopic measurements of all steps.

Integrated age error calculated by quadratically combining errors of isotopic measurements of all steps.

Plateau age is inverse-variance-weighted mean of selected steps.

Plateau age error is inverse-variance-weighted mean error (Taylor, 1982) times root MSWD where MSWD>1.

Plateau error is weighted error of Taylor (1982).

Decay constants and isotopic abundances after Steiger and Jäger (1977).

"X" preceding sample ID denotes analyses excluded from plateau age calculations.

Weight percent K_2O calculated from ^{39}Ar signal, sample weight, and instrument sensitivity.

Ages calculated relative to FC-2 Fish Canyon Tuff sanidine interlaboratory standard at 28.02 Ma

Decay Constant (λK (total)) = 5.543e-10/a

Correction factors:

($^{39}Ar/^{37}Ar$)Ca = 0.00068 ± 2e-05

($^{36}Ar/^{37}Ar$)Ca = 0.00028 ± 1e-05

($^{38}Ar/^{39}Ar$)K = 0.0125

($^{40}Ar/^{39}Ar$) = 0 ± 0.0004

sample AR-1 (Fig. 7) range from unzoned (grains 1, 18, 22), have oscillatory zonation (grains 5, 21, 23), or have extremely complex zoning (grains 10, 11, 24, 28). Some cores from sample AR-2 (Fig. 8) are unzoned (grains 1, 17) but generally have oscillatory zonation (grains 5, 10, 12, 13). The cores from sample AR-5 (Fig. 8) are bright in CL and are surrounded by a thin, dark CL zone. The rims of all of the samples are low U and are typically ~20-40 mm in width. We dated both rims and cores from each sample except AR-3, which only yielded one zircon (Fig. 8).

The rim dates from these zircons (Fig. 9) had U concentrations ranging from ~16 ppm to ~450 ppm and all had high amounts of common Pb, with the percentage of ^{206}Pb that was common ranging from ~5% to ~70% (Table 4). For these dates, which were <20 Ma, we used the Tera-Wasserburg concordia intercept ages. The dates using the measured U-Pb ratios were 9.8 ± 1.7 Ma for sample AR-1 and 11.0 ± 2.2 Ma for sample AR-5. The Tera-Wasserburg intercept age using the combined data from three samples (AR-1, AR-2, and AR-5) is 10.4 ± 1.1 Ma. If the $^{238}U/^{206}Pb$ ages corrected for common Pb are used, the weighted mean of all three samples is 10.3 ± 1.0 Ma.

Two zircons yielded Phanerozoic ages. Sample AR-1 had a $^{238}U/^{206}Pb$ date from the rim of 96 ± 2 Ma but the CL image indicates that the beam may have overlapped part of the core of the grain, which would make this an average age of two zones with different ages. The other analysis, from sample AR-5, appears to be entirely within the rim zone, and yields a $^{238}U/^{206}Pb$ date of 20 ± 1 Ma, but a date on the opposite tip of the same grain was 9 ± 3 Ma, so we suggest that both of these dates may be problematic.

The core ages from all of the samples were Proterozoic. The total age range for the cores is ~1250 Ma to ~1700 Ma (n=25).

TABLE 4. Complete u/Pb zircon data collected by SHRIMP

Sample	Spot[a]	% comm ^{206}Pb[b]	U (ppm)	Th (ppm)	Th/U	$^{207}Pb^{c}/^{235}U$	% err	$^{206}Pb^{c}/^{238}U$	% err	err corr.[d]	$^{238}U^{e}/^{206}Pb$-tot.	% err	$^{207}Pb^{e}/^{206}Pb$-tot.	% err	$^{207}Pb^{c}/^{206}Pb$	% err	$^{206}Pb/^{238}U$ age (Ma)	± 1s (Ma)	$^{207}Pb/^{206}Pb$ age (Ma)f	± 1s (Ma)	%conc.[g]	Standard[h]
Phanerozoic Ages																						
AR1	18.2	23.8	193	134	0.7						559.8	5	0.0874	16			11	0.613				RG6
AR1	22.1	10.6	131	83	0.6						559.7	5	0.2346	9			9	0.653				RG6
AR1	17.1	22.9	258	256	1.0						558.9	4	0.1728	11			10	0.51				RG6
AR1	21.1	5.2	227	81	0.4						455.2	3	0.2337	11			11	0.588				RG6
AR1	16.1	8.6	52	164	3.1						420.5	5	0.1602	20			13	0.893				RG6
AR2	10.1	19.5	32	8	0.3						821.8	9	0.1999	25			6	0.804				RG6
AR2	1.1	68.3	16	4	0.2						652.0	7	0.1297	14			9	0.637				RG6
AR5	2.1	16.0	109	26	0.2						554.6	5	0.2272	18			9	0.823				R33
AR5	6.1	23.7	162	72	0.4						476.9	10	0.1142	35			12	1.443				R33
AR5	14.1	21.0	256	79	0.3						435.2	3	0.2123	13			12	0.619				R33
AR5	4.2	14.4	147	50	0.3						239.3	7	0.5861	11			9	3.277				R33
AR1	5.1	3.3	453	142	0.3	0.12	14.8	0.0152	2.2	0.15	64.5	2	0.0740	7	0.0593	15	96	2.038				RG6
AR5	4.1	5.9	132	58	0.4	0.03	40.9	0.0032	3.3	0.08	297.2	3	0.0928	24	0.0663	41	20	0.835				R33
Proterozoic Ages																						
AR1	5.2	4.4	400	112	0.3	0.63	4.7	0.0541	1.5	0.31	18.4	1	0.0887	3	0.0850	5	326	5	1315	87	25	RG6
AR1	1.2	2.1	152	71	0.5	2.09	5.0	0.1757	1.8	0.37	5.7	2	0.0909	3	0.0862	5	1029	19	1343	90	77	RG6
AR1	7.1	3.8	1394	554	0.4	1.03	4.3	0.0849	1.1	0.25	11.8	1	0.0882	4	0.0884	4	506	6	1390	80	36	RG6
AR1	28.1	<0.1	815	69	0.1	3.08	1.1	0.2524	1.0	0.89	4.0	1	0.0888	1	0.0885	1	1455	14	1393	10	104	RG6
AR1	22.2	4.3	1212	432	0.4	0.86	2.2	0.0698	1.1	0.48	14.3	1	0.0897	2	0.0897	2	417	5	1418	38	29	RG6
AR1	23.1	1.0	599	133	0.2	2.65	1.3	0.2138	1.1	0.83	4.7	1	0.0902	1	0.0900	1	1238	13	1425	14	87	RG6
AR1	12.1	3.0	814	1002	1.2	1.72	1.7	0.1384	1.1	0.62	7.2	1	0.0914	1	0.0904	1	813	9	1433	26	57	RG6
AR1	11.1	3.1	1921	1544	0.8	1.85	2.1	0.1449	1.8	0.89	6.9	2	0.0926	1	0.0925	1	848	15	1477	18	57	RG6
AR1	24.1	4.3	1164	319	0.3	1.09	1.4	0.0855	1.1	0.76	11.7	1	0.0925	1	0.0928	1	507	6	1483	18	34	RG6
AR1	10.1	3.6	1136	332	0.3	1.61	3.3	0.1246	1.1	0.32	8.0	1	0.0930	3	0.0935	3	731	9	1497	58	49	RG6
AR1	14.1	1.7	1504	1671	1.1	3.01	1.5	0.2243	1.0	0.69	4.5	1	0.0978	1	0.0975	1	1285	13	1577	21	82	RG6
AR1	4.1	4.6	369	158	0.4	1.49	5.0	0.1104	2.9	0.58	9.0	3	0.0990	4	0.0982	4	646	19	1589	76	41	RG6
AR1	20.1	5.0	1354	236	0.2	1.22	2.4	0.0900	1.1	0.44	11.1	1	0.0985	2	0.0985	2	529	7	1596	41	33	RG6
AR1	18.1	3.3	738	419	0.6	2.39	3.2	0.1749	2.0	0.61	5.7	2	0.1003	3	0.0992	3	1009	20	1609	48	63	RG6
AR2	12.1	0.9	1110	104	0.1	2.42	1.9	0.2019	1.0	0.54	5.0	1	0.0868	2	0.0869	2	1176	12	1358	30	87	RG6
AR2	13.1	2.9	113	53	0.5	2.05	3.4	0.1687	1.7	0.50	5.9	2	0.0967	2	0.0880	3	987	17	1383	57	71	RG6
AR2	17.1	1.8	128	29	0.2	2.13	6.1	0.1727	4.7	0.77	5.8	5	0.0875	4	0.0894	4	1008	46	1412	75	71	RG6
AR2	5.1	0.5	129	20	0.2	3.00	8.1	0.2391	6.6	0.82	4.2	7	0.0922	4	0.0909	5	1377	88	1445	89	95	RG6
AR2	18.1	4.9	349	145	0.4	1.92	7.2	0.1322	1.2	0.16	7.6	1	0.1050	7	0.1051	7	763	12	1716	131	44	RG6
AR3	2.1	<0.1	970	24	0.02	3.38	1.6	0.2717	1.6	0.97	3.7	2	0.0905	0	0.0903	0	1560	24	1432	7	109	RG6
AR5	11.1	4.5	123	58	0.5	0.32	7.3	0.0281	1.3	0.18	35.4	1	0.0854	6	0.0825	7	172	3	1259	140	14	R33
AR5	7.1	2.3	198	81	0.4	1.64	2.6	0.1415	0.8	0.32	7.0	1	0.0863	2	0.0841	3	836	7	1295	49	65	R33
AR5	9.1	4.0	432	134	0.3	1.01	6.5	0.0834	4.0	0.61	12.0	4	0.0900	5	0.0883	5	497	19	1388	98	36	R33
AR5	16.1	2.3	173	67	0.4	2.47	3.7	0.1889	0.8	0.21	5.3	1	0.0948	4	0.0948	4	1092	9	1525	69	72	VP-10
AR5	8.1	0.5	894	554	0.6	3.96	0.5	0.2811	0.3	0.59	3.6	0	0.1024	0	0.1022	0	1591	4	1664	7	96	VP-10

a) Analyses are listed in increasing age. All localities are in UTM coordinates using the NAD27 CONUS datum.

b) Common Pb component (%) of total ^{206}Pb, determined using measured ^{204}Pb

c) Ratio was corrected for common Pb using measured ^{204}Pb; ratios not given for samples with ages <100 Ma because of low precision

d) Error Correlation coefficient

e) "tot" = total, uncorrected ratios

f) $^{207}Pb/^{206}Pb$ ages are not included for samples <100 Ma because of low precision

g) Concordance (%) = (^{206}Pb-^{238}U age)/(^{206}Pb-^{207}Pb age) *100; only given for samples older than 100 Ma

h) SHRIMP standard ages: R33=420 Ma; RG6=1440 Ma; VP10=1200 Ma

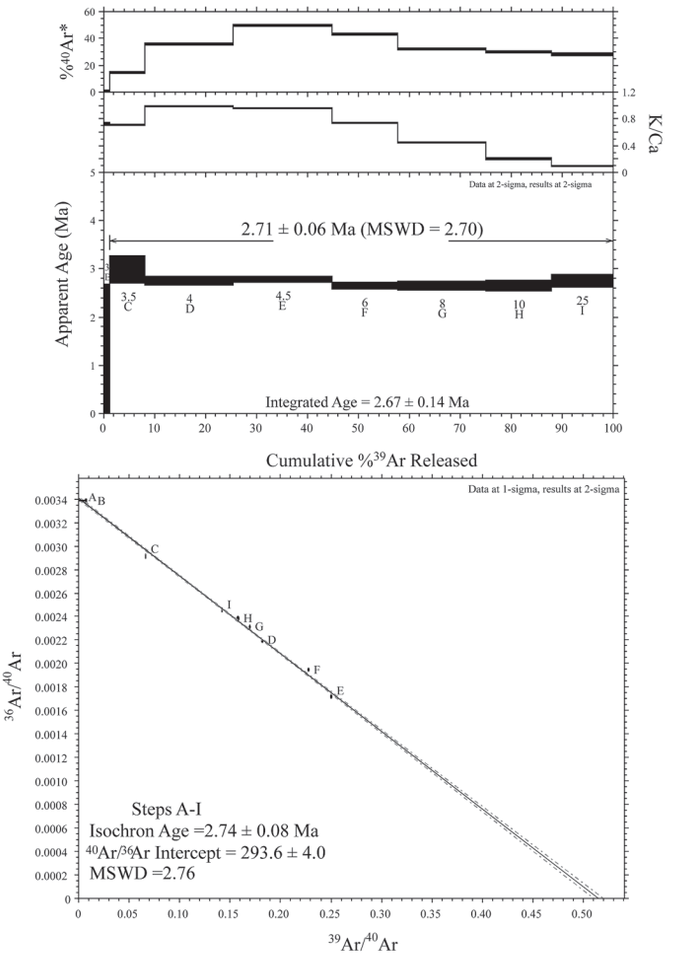


FIGURE 6. 40Ar/39Ar (A) age spectra and (B) isochron from the groundmass concentrate from sample AR-8, the host basalt. Errors are quoted at 2σ. MSWD is the mean square of weighted deviates.

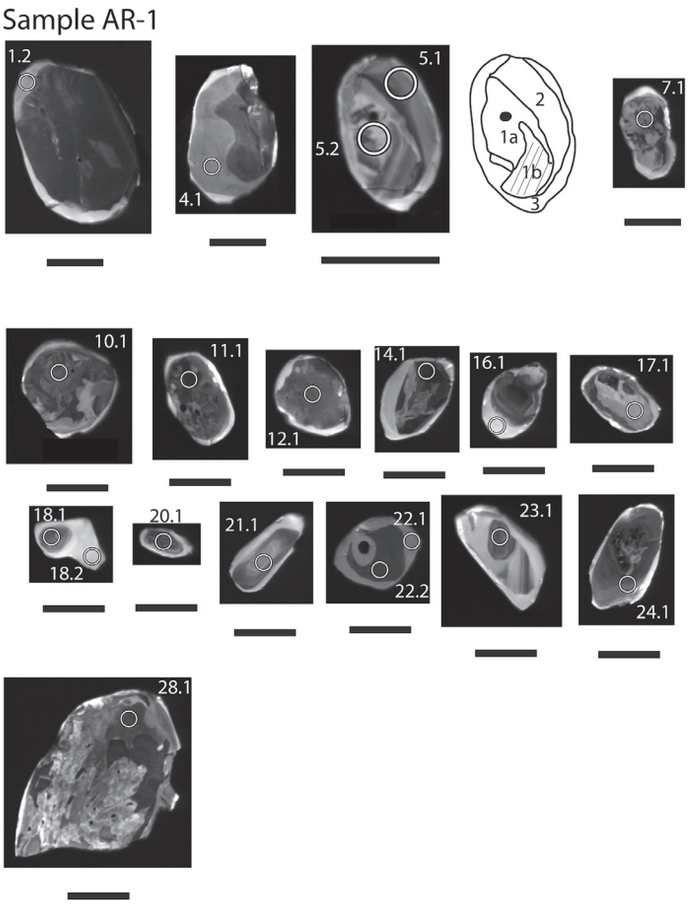


FIGURE 7. Cathodoluminescence images of zircons from sample AR-1. Analytical spot size and location is approximated by the circles on each image. Scale bar beneath each image is 100 μm. Lighter parts of each image indicate lower U concentrations than the darker areas. Grain 5 has a line drawing that shows two zones from within the core, an unzoned section (1a) with a dark inclusion, and an oscillatory zoned section (1b), surrounded by two outer layers, zone 2 and a thin zone 3 that was too thin to date with a 30 μm beam diameter.

When plotted on a relative probability distribution diagram, which takes into consideration the total number of ages as well as their uncertainties, the main peaks are at 1430 Ma, 1480 Ma, and 1665 Ma.

Many analyses had high common Pb and high U concentrations and most are discordant, with some that are only 14% concordant. Th/U was generally low. Three analyses have Th/U of 0.8-1.2, and about half of the total analyses are ≥0.4, generally consistent with typical values of ~0.5 or greater for this ratio in igneous zircon (Hoskin and Schaltegger, 2003). The remaining analyses have Th/U <0.4 and this is typical of metamorphic zircon growth. In the ages from 1700–1400 Ma, there is a weak correlation between decreasing age and decreasing Th/U. For ages younger than 1400 Ma, the Th/U slightly increases with decreasing age. Numerous analyses with excessive reverse discordance and high common Pb were discarded.

DISCUSSION

Although bulk compositions for the xenoliths were not analyzed because they were too small and the entire sample was crushed for zircon extraction, the protolith compositions can be approximated based on mineralogy and abundance of mafic minerals. The most mafic sample is AR-4. This sample is likely a diorite based on the >50% mafic mineral content, the lack of K-feldspar, and the presence of plagioclase + quartz. A mafic to intermediate composition is also indicated by the lack of zircon and the more Mg-rich pyroxene and more Ca-rich plagioclase relative to sample AR-3. Samples AR-1, AR-2, and AR-3 are felsic as indicated by the presence of K-feldspar in addition to plagioclase and quartz, and this assemblage suggests that the protolith was likely a granite. None of the samples had garnet, thus precluding the estimation of the pressures at which the xenoliths resided prior to eruption (e.g., Lee et al., 1993). However, the mineralogy is consistent with felsic to intermediate igneous protoliths that have resided at lower crustal pressure and temperature conditions prior to entrainment in the host basalt.

The new date of basalt magmatism at 2.71 ± 0.06 Ma from the Elephant Butte field is generally consistent with previous K-Ar

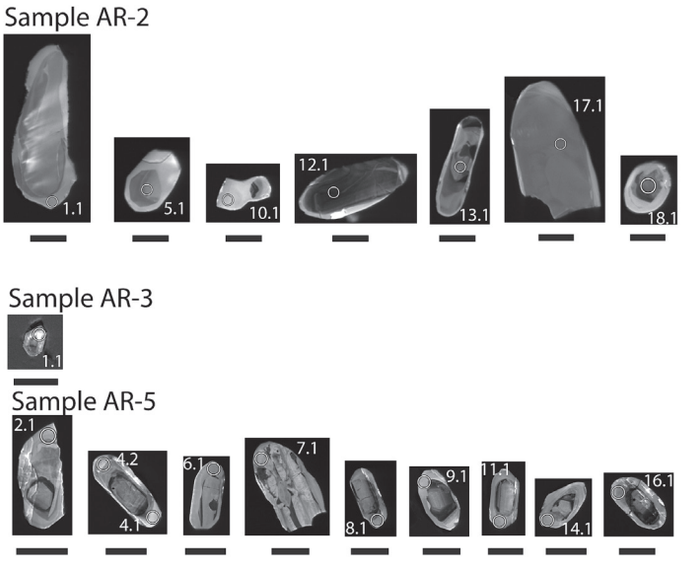


FIGURE 8. Cathodoluminescence images of zircons from samples AR-2, AR-3, and AR-5. Analytical spot size and location is approximated by the circles on each image. Scale bar beneath each image is 100 μm. Lighter parts of each image indicate lower U concentrations than the darker areas.

dates suggesting a range of 3-2 Ma for the lava flows (Bachman and Mehnert, 1978). This new date is more precise than previous work and further dates on other flows would provide a reliable duration of magmatism at this eruptive center. These dates would then help constrain the timing of extension within the Cutter Sag transfer zone (Mack and Seager, 1995).

The ages of the zircon cores within the xenoliths, though generally imprecise, confirm ages determined from the Proterozoic rocks exposed on the surface in southern New Mexico, particularly those in the nearby Caballo Mountains. (Amato and Becker, thiseguidebook). The few ages around 1660 Ma are representative of Mazatzal province crust (Karlstrom et al., 2004; Amato et al., 2008; 2011), but it is unclear if these ages are xenocrystic zircons within ~1.4 Ga granite protoliths or if the rocks themselves are actually 1.6 Ga in age. Sample AR-5 has the most precise date in this age range, at 1664 ± 14 Ma, but the other four analyses from the same sample have $^{207}Pb/^{206}Pb$ ages ranging from 1525–1260 Ma all with large uncertainties. The possibilities for this age range include: (1) the protolith is sedimentary and the zircons are detrital, with a depositional age younger than ~1.25 Ga; (2) the protolith is igneous, with an intrusive age of ~1.25 Ga and inherited zircons in the 1.6–1.4 Ga age range; (3) the protolith is igneous with an intrusive age of 1.66 Ga and the imprecise, younger, highly discordant ages represent Pb-loss events or mixed ages between growth zones. Based on the single, precise, nearly concordant 1.66 Ga analysis, we suggest that the protolith age was 1664 ± 14 Ma and that the other ages are not significant.

Similar issues with discordance and possible Pb-loss likely affect sample AR-2. This sample has one zircon at 1716 ± 262 Ma but the low precision precludes interpretation as it could be part of either the Mazatzal province basement or the ~1.4 Ga suite. The other four grains have $^{207}Pb/^{206}Pb$ dates ranging from 1.45–1.35 Ga and thus this protolith is likely a granite associated with the ~1.4 Ga suite. The $^{207}Pb/^{206}Pb$ ages of this sample decrease with increasing discordance, suggesting Pb-loss events that have occurred long before the present, thus adding to the complexity of the interpretation.

Sample AR-3 had only one analysis, and although it is reversely discordant, the precise 1432 ± 14 Ma age is probably the crystallization age of the protolith.

Sample AR-1 had the most zircon analyses and many had similar issues as the others with strong discordance. A weighted mean of all of the data is 1446 ± 38 Ma but a high MSWD (8.5) indicates that these dates comprise multiple populations. The zircons with ages between 1.5–1.3 Ga yield an age of 1452 ± 32 Ma (MSWD=2.1), and if this is the intrusive age of the protolith, as we suggest, then the older zircons would be inherited grains and the younger zircons would reflect Pb loss.

Together, it appears that one of the xenoliths represents ~1.65 Ga Mazatzal age crust, and the other four samples are representative of the ~1.45 Ga granitic intrusive suite that makes up the majority of the exposed Proterozoic basement in southern New Mexico. Given that (1) the crustal thickness in this part of New Mexico is 30–35 km thick (Keller et al., 1979; Wilson et al., 2005b); (2) granulite xenoliths were inferred to originate from 29-36 km depth based on geothermometry (Warren et al., 1979); and (3) ~1.45 Ga granites are common in surface exposures of Proterozoic rock, the total volume of ~1.4 Ga granites in the lower, middle, and upper crust in the southern Mazatzal province is impressively large.

The rim ages from the xenolith zircons suggest significant heating occurred in the lower crust around 10 Ma. This age was determined using both the Tera-Wasserburg intercept age using ratios uncorrected for common Pb as well as the $^{238}U/^{206}Pb$ ages corrected for common Pb. Both techniques yield dates of about 10.5 ± 1 Ma. This is the same age as the renewed onset of Rio Grande rifting and magmatism following a ~10 m.y. hiatus (Seager et al., 1984). The only known magmatism in the southern Rio Grande rift of this age is the Selden basalt, dated using the K-Ar method at 9.6 Ma. This flow is 80 km south of the study area and 65 km south of the southernmost Elephant Butte volcanic field lava flows. Thus, it appears that upwelling mantle heating associated with rifting at 10 Ma did not everywhere yield surface flows, but the heating was sufficient to grow new zircon over older cores within the samples that were incorporated into erupted basalts at 2.7 Ma. Perhaps this heating was caused by basaltic melts that underplated the crust but did not ascend to the surface because the amount of extension at this latitude was insufficient to create pathways to the surface, whereas the 2.7 Ma rifting within the Cutter Sag transfer zone did allow voluminous basaltic volcanism to occur.

CONCLUSIONS

Xenoliths with the Elephant Butte volcanic field are granulite-facies metamorphic rocks with protoliths that include both ~1.65 Ga Mazatzal province crust and ~1.45 Ga granites that are part

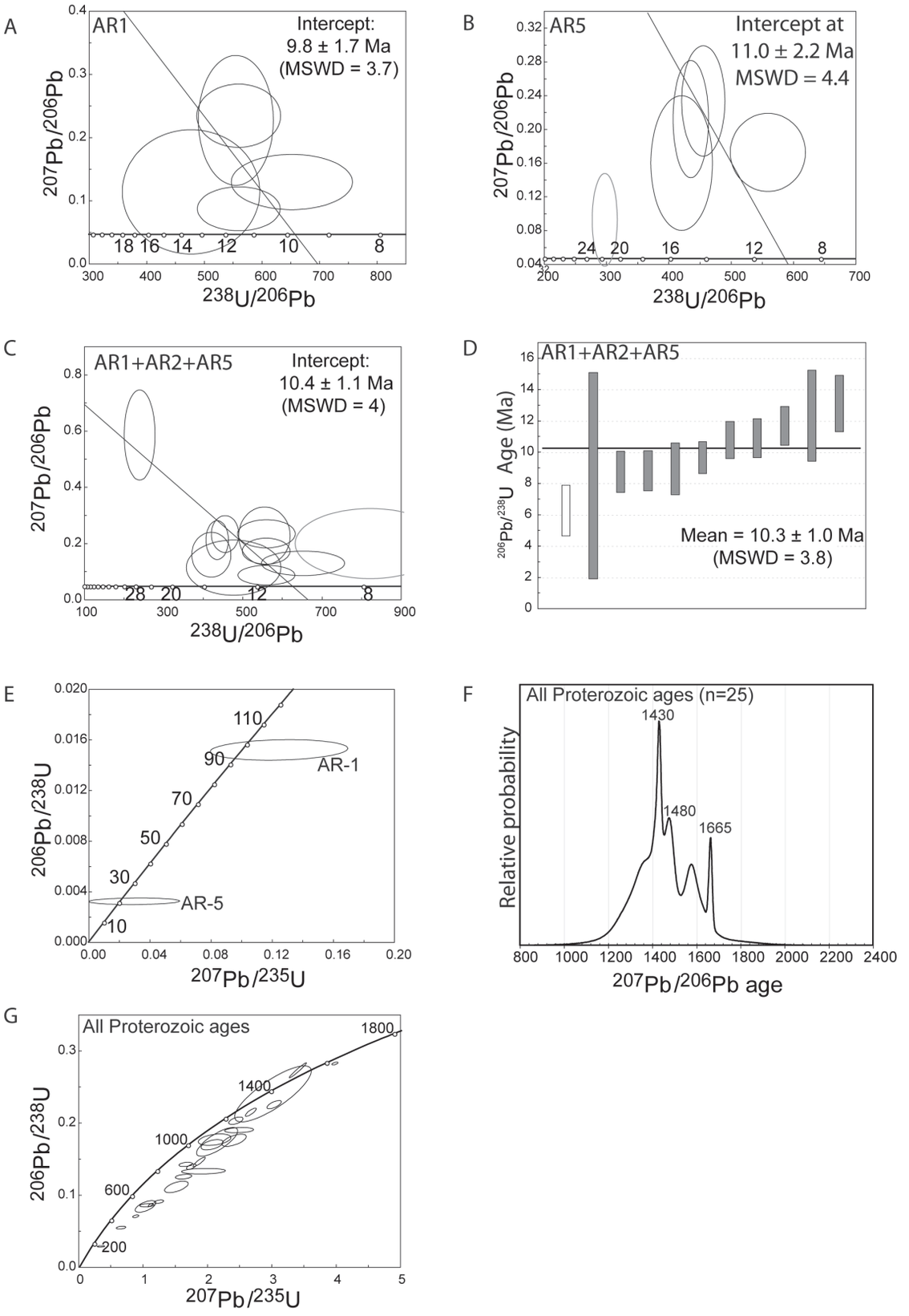


FIGURE 9. Geochronology data shown on weighted mean plots and standard concordia plots, created using Isoplot 3.6 (Ludwig, 2008). Tera-Wasserburg concordia plots for samples (A) AR-1, (B) AR-5, and (C) combined data from AR1, AR2, and AR5. (D) weighted mean of the 238U/206Pb ages corrected for common Pb. (E) conventional concordia diagram for two analyses; (F) Relative probability distribution diagram for all Proterozoic ages; and (G) conventional concordia diagram for all Proterozoic ages, showing extensive discordance.

of a continent-wide suite of felsic magmatism. Zircons from the xenoliths have cores with both oscillatory zonation and others with textures suggesting extreme alteration. These cores generally have high common Pb and ages that are highly discordant. Zircon rims have low U, high common Pb, and U-Pb SHRIMP dating suggest that they grew at 10 ± 1 Ma. We suggest that heating at this time was caused by mantle upwelling that accompanied renewed extension at 10 Ma after an 8 m.y. hiatus. This extension and heating did not result in surface eruptions, although eruption of the Selden basalt >65 km to the south was coeval. Eruptions at 2.71 ± 0.6 Ma, based on $^{40}Ar/^{39}Ar$ dating of the host basalt, occurred in a transfer zone of the Rio Grande rift that allowed basaltic magmas to ascend to the surface where they lie unconformably on Cretaceous sandstones.

ACKNOWLEDGMENTS

The Armendaris Ranch gave permission to collect samples on the property. The SHRIMP data were collected at the Stanford/U.S.G.S. facility at Stanford University and this was made possible by Joe Wooden. Frank Mazdab helped acquire the CL images. Lynn Heizler and Nelia Dunbar assisted with the electron microprobe data collection. The New Mexico Geological Society provided funding to Carmen Athens, who worked on this study as part of an undergraduate research project at New Mexico State University. Greg Mack and Ben Duval assisted in the sampling. Discussions with Greg Mack and Nancy McMillan on the history of rifting and rift magmatism are appreciated. Jorge Vasquez and Axel Schmitt provided insight on the interpretation of the young U-Pb dates. This paper benefitted from reviews by Shari Kelley and Nancy McMillan.

REFERENCES

Amato, J.M. and Becker, T., this guidebook, Proterozoic Rocks of the Caballo Mountains and Kingston mining district: U-PbGeochronology and correlations within the Mazatzal Province of Southern New Mexico: New Mexico Geological Society, this Field Conference Guidebook.

Amato, J.M., Boullion, A.O., Serna, A.M., Sanders, A.E., Farmer, G.L., Gehrels, G.E., and Wooden, J.L., 2008, The evolution of the Mazatzal province and the timing of the Mazatzal orogeny: Insights from U-Pb geochronology and geochemistry of igneous and metasedimentary rocks in southern New Mexico: Geological Society of America Bulletin, v. 120, p. 328-346.

Amato, J.M., Heizler, M.T., Boullion, A.O., Sanders, A.E., Toro, J., McLemore, V.T., and Andronicos, C.L., 2011, Syntectonic 1.46 Ga magmatism and rapid cooling of a gneiss dome in the southern Mazatzal Province: Burro Mountains, New Mexico: Geological Society of America Bulletin, v. 123, p. 1720-1744.

Anderson, J.L., 1989, Proterozoic anorogenic granites of the southwestern United States, in Jenney, J.P., and Reynolds, S.J., eds., Geologic Evolution of Arizona: Tucson, Arizona Geological Society Digest 17, p. 211-238.

Anderson, J.L., and Morrison, J., 2005, Ilmenite, magnetite, and peraluminous Mesoproterozoic anorogenic granites of Laurentia and Baltica: Lithos, v. 80, p. 45-60.

Anthony, E.Y., and Poths, J., 1992, ^{3}He surface exposure dating and its implications for magma evolution in the Potrillo volcanic field, Rio Grande rift, New Mexico, USA: Geochimica et Cosmochimica Acta, v. 56, p. 4105-4108.

Bachman, G.O., and Mehnert, H.H., 1978, New K-Ar dates and the late Pliocene to Holocene geomorphic history of the central Rio Grande region, New Mexico: Geological Society of America Bulletin, v. 89, p. 283-292.

Baldridge, W.S., 2004, Pliocene-Quaternary volcanism in New Mexico and a model for genesis of magmas in continental extension, in Mack, G.H., and Giles, K.A., eds., The Geology of New Mexico: A Geologic History: New Mexico Geological Society, Special Publication 11, p. 313-330.

Berglund, H.T., Sheehan, A.F., Murray, M.H., Roy, M., Lowry, A.R., Nerem, R.S., and Blume, F., 2012, Distributed deformation across the Rio Grande Rift, Great Plains, and Colorado Plateau: Geology, v. 40, p. 23-26.

Chapin, C.E., 1971, The Rio Grande rift, part I: modifications and additions, N. M. Geological Society, 22nd Field Conference Guidebook, p. 191-201.

Dunbar, N.W., 1999, Cosmogenic ^{36}Cl-determined age of the Carrizozo lava flows, south-central New Mexico: New Mexico Geology, v. 21, p. 25-29.

Hamblock, J.M., Andronicos, C.L., Miller, K.C., Barnes, C.G., Ren, M.-H., Averill, M.G., and Anthony, E.Y., 2007, A composite geologic and seismic profile beneath the southern Rio Grande rift, New Mexico, based on xenolith mineralogy, temperature, and pressure: Tectonophysics, v. 442, p. 14-48.

Hanchar, J.M., Miller, C.F., Wooden, J.L., Bennett, V.C., and Staude, J.-M.G., 1994, Evidence from xenoliths for a dynamic lower crust, eastern Mojave desert, California: Journal of Petrology, v. 35, p. 1377-1415.

Hanchar, J.M., and Rudnick, R.L., 1995, Revealing hidden structures: The application of cathodoluminescence and back-scattered electron imaging to dating zircon from lower crustal xenoliths: Lithos, v. 36, p. 289-303.

Harrison, R.W., and Cather, S.M., 2004, The Hot Springs fault system of south-central New Mexico - evidence for the northward translation of the Colorado Plateau during the Laramide orogeny: New Mexico Bureau of Geology and Mineral Resources, Bulletin 160, p. 161-179.

Henry, C.D., and Price, J.G., 1986, Early Basin and Range development in Trans-Pecos Texas and adjacent Chihuahua: Magmatism and orientation, timing, and style of extension: Journal of Geophysical Research, v. 91, p. 6213-6224.

Hoskin, P.W.O., and Schaltegger, U., 2003, The composition of zircon and igneous and metamorphic petrogenesis, in Hanchar, J.M., and Hoskin, P.W.O., eds., Reviews in Mineralogy and Geochemistry Volume 53: Zircon, Volume 53: Washington, D.C., Mineralogical Society of America, p. 27-62.

Karlstrom, K.E., Amato, J.M., Williams, M.L., Heizler, M., Shaw, C.A., Read, A.S., and Bauer, P., 2004, Proterozoic tectonic evolution of the New Mexico region: A synthesis, in Mack, G.H., and Giles, K.A., eds., The Geology of New Mexico: A Geologic History: New Mexico Geological Society, Special Publication 11, p. 1-34.

Karlstrom, K.E., and Bowring, S.A., 1988, Early Proterozoic assembly of tectonostratigraphic terranes in southwestern North America: Journal of Geology, v. 96, p. 561-576.

Kay, R.W., and Kay, S.M., 1981, The nature of the lower continental crust: Inferences from geophysics, surface geology, and crustal xenoliths: Reviews of Geophysics, v. 19, p. 271-297.

Keller, G.R., Braile, L.W., and Schlue, J.W., 1979, Regional crustal structure of the Rio Grande rift from surface wave dispersion measurements, in Riecker, R.E., ed., Rio Grande Rift: Tectonics and Magmatism: Washington, D. C., American Geophysical Union, p. 115-126.

Keller, G.R., Morgan, P., and Seager, W.R., 1991, Crustal structure, gravity anomalies and heat flow in the southern Rio Grande rift and their relationship to extensional tectonics: Tectonophysics, v. 174, p. 21-37.

Kelley, V.C., and Silver, C., 1952, Geology of the Caballo Mountains: Albuquerque, New Mexico, University of New Mexico Publications in Geology, no. 4, 286 p.

Lee, D.-C., Halliday, A.N., Hunter, R.H., Holden, P., and Upton, B.G.J., 1993, Rb-Sr and Sm-Nd isotopic variations in dissected crustal xenoliths: Geochimica et Cosmochimica Acta, v. 57, p. 219-230.

Li, Y., Barnes, M., Chattopadhyay, I., Barnes, C., and Frost, C., 2004, U-Pb zircon ages of surface and subsurface samples from Texas and southern New Mexico: Implications for Grenville-age and Tertiary magmatism (abstr.): Geological Society of America, Abstracts with Programs, v. 36, p. 147.

Liati, A., and Gebauer, D., 2002, U-Pb SHRIMP-dating of zircon domains from xenoliths of the Rio Grande Rift (Kilbourne Hole)(abstr,): implications for the timing of mantle events: Goldschmidt Conference Abstracts, p. A455.

Lozinsky, R.P., 1986, Geology and late Cenozoic history of the Elephant Butte area, Sierra County, New Mexico: New Mexico Bureau of Mines and Mineral Resources, Circular, v. 187, p. 1-40.

Ludwig, K.R., 2008, Isoplot/Ex 3.6: A geochronologic toolkit for Microsoft Excel: Berkeley, California, Berkeley Geochronology Center Special Publication No. 4, 77 p.

Mack, G.H., 2004, Middle and late Cenozoic crustal extension, sedimentation, and volcanism in the southern Rio Grande rift, Basin and Range, and south-

ern transition zone of southwestern New Mexico, in Mack, G.H., and Giles, K.A., eds., The Geology of New Mexico: A Geologic History: New Mexico Geological Society, Special Publication 11, p. 389-406.

Mack, G.H., and Seager, W.R., 1995, Transfer zones in the southern Rio Grande rift: Journal of the Geological Society, v. 152, p. 551-560.

McMillan, N.J., Dickin, A.P., and Haag, D., 2000, Evolution of magma source regions in the Rio Grande rift, southern New Mexico: Geological Society of America Bulletin, v. 112, p. 1582-1593.

Nelson, E.P., and Hunter, J., 1986, Laramide thin-skinned deformation in Permian rocks, Fra Cristobal Range, south-central New Mexicn: N. M. Geological Society, 37th Field Conference Guidebook, p. 115-121.

Nielsen, H., and Sigurdsson, H., 1981, Quantitative methods for electron microprobe analysis of sodium in natural and synthetic glasses: American Mineralogist, v. 66, p. 547-552.

Padovani, E.R., and Carter, J.L., 1977, Aspects of the deep crustal evolution beneath south central New Mexico, in Heacock, J.G., ed., The Earth's Crust, American Geophysical Union Monograph 20, p. 19-55.

Perry, F.V., Baldridge, W.S., and DePaolo, D.J., 1987, Role of asthenosphere and lithosphere in the genesis of late Cenozoic basaltic rocks from the Rio Grande rift and adjacent regions of the southwestern United States: Journal of Geophysical Research, v. 92, p. 9193-9213.

Renne, P.R., Swisher, C.C., Deino, A.L., Karner, D.B., Owens, T.L., and DePaolo, D.J., 1998, Intercalibration of standards, absolute ages and uncertainties in ^{40}Ar-^{39}Ar dating: Chemical Geology, v. 145, p. 117-152.

Sanudo-Wilhelmy, S.A., and Flegal, A.R., 1994, Temporal variations in lead concentrations and isotopic composition in the Southern California Bight: Geochimica et Cosmochimica Acta, v. 58, p. 3315-3320.

Scherer, E.E., Cameron, K.L., Johnson, C.M., Beard, B.L., Barovich, K.M., and Collerson, K.D., 1997, Lu-Hf geochronology applied to dating Cenozoic events affecting lower crustal xenoliths from Kilbourne Hole, New Mexico: Chemical Geology, v. 142, p. 63-78.

Schmitt, A.K., Grove, M., Harrison, T.M., Lovera, O., Hulen, J., and Walters, M., 2003, The Geysers - Cobb Mountain Magma System, California (Part 1): U-Pb zircon ages of volcanic rocks, conditions of zircon crystallization and magma residence times: Geochimica et Cosmochimica Acta, v. 67, p. 3423-3442.

Schmitt, A.K., and Hulen, J.B., 2008, Buried rhyolites within the active, high-temperature Salton Sea geothermal system: Journal of Volcanology and Geothermal Research, v. 178, p. 708-718.

Seager, W.R., Shafiqullah, M., Hawley, J.W., and Marvin, R.F., 1984, New K-Ar dates from basalts and the evolution of the southern Rio Grande rift: Geological Society of America Bulletin, v. 95, p. 87-99.

Steiger, R.H., and Jäger, E., 1977, Subcommission on Geochronology: Convention on the use of decay constants in geo- and cosmochronology: Earth and Planetary Science Letters, v. 36, p. 359-362.

Taylor, J.R., 1982, An Introduction to Error Analysis: The Study of Uncertainties in Physical Measurements: Mill Valley, California, University Science Books, 270 p.

Thompson, S., 1955a, Geology of the Fra Cristobal Rango: N. M. Geological Society, 6th Field Conference Guidebook, p. 155-157.

Thompson, S., III, 1955b, Geology of the southern part of the Fra Cristobal Range, Sierra County, New Mexico [M.S. thesis]: Albuquerque, University of New Mexico.

Warren, R.G., Kudo, A.M., and Keil, K., 1979, Geochemistry of lithic and single-crystal inclusions in basalt and a characterization of the upper mantle-lower crust in the Engle Basin, Rio Grande rift, New Mexico, in Riecker, R.E., ed., Rio Grande rift: Tectonics and magmatism: Washington, D. C., American Geophysical Union, p. 393-415.

Wilson, D., Aster, R., Ni, J., Grand, S., West, M., Gao, W., Baldridge, W.S., and Semken, S., 2005a, Imaging the seismic structure of the crust and upper mantle beneath the Great Plains, Rio Grande Rift, and Colorado Plateau using receiver functions: Journal of Geophysical Research, v. 110, p.

Wilson, D., Aster, R., West, M., Ni, J., Grand, S., Gao, W., Baldridge, W.S., and Semken, S., 2005b, Lithospheric structure of the Rio Grande rift: Nature, v. 433, p. 851-855.